

CONTROL-VOLUME MIXED FINITE ELEMENT METHODS

J. E. JONES*

ICASE

NASA Langley Research Center
Hampton, VA 23681-0001

Z. CAI

Center for Applied Mathematics
Purdue University
West Lafayette, IN 47907-1395

S. F. MCCORMICK

Department of Applied Mathematics
University of Colorado at Boulder
Boulder, CO 80309-0526

T. F. RUSSELL

Department of Mathematics
University of Colorado at Denver
Campus Box 170
Denver, CO 80217-3364

Abstract

A key ingredient in simulation of flow in porous media is accurate determination of the velocities that drive the flow. Large-scale irregularities of the geology (faults, fractures, and layers) suggest the use of irregular grids in simulation. This paper presents a control-volume mixed finite element method that provides a simple, systematic, easily implemented procedure for obtaining accurate velocity approximations on irregular block-centered grids. The control-volume formulation of Darcy's law can be viewed as a discretization into element-sized "tanks" with imposed pressures at the ends, giving a local discrete Darcy law analogous to the block-by-block conservation in the usual mixed discretization of the mass-conservation equation. Numerical results in two dimensions show second-order convergence in the velocity, even with discontinuous anisotropic permeability on an irregular grid. The method extends readily to three dimensions.

*This research was supported in part by the National Aeronautics and Space Administration under NASA Contract No. NAS1-19480 while the first author was in residence at the Institute for Computer Applications in Science and Engineering (ICASE), NASA Langley Research Center, Hampton, VA 23681-0001

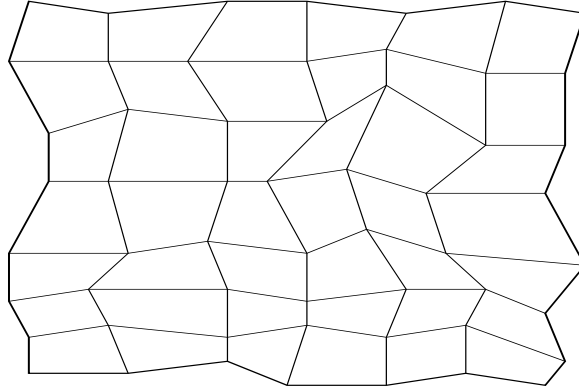


Figure 1: Logically rectangular grid of irregular quadrilaterals

1 Introduction

As techniques of reservoir description become more sophisticated, it becomes increasingly important to model flows of reservoir fluids accurately. In particular, it is desirable to accurately represent large-scale irregularities of reservoir geology in models. The control-volume mixed finite element method allows the use of irregular grids while maintaining many of the familiar properties of block-centered finite difference methods for rectangular grids. For example, it preserves the notion of block-by-block material balance, with physical interblock-flow terms. It also yields an analogue of the local discrete Darcy law (relating a combination of fluxes to a pressure drop between blocks) on a block-sized “tank” between two pressure nodes. The method can be applied to any “logically rectangular” grid of irregular quadrilaterals in two dimensions, or analogous hexalaterals in three dimensions. In two dimensions, “logically rectangular” means that each grid block can be assigned an index (i, j) such that it shares an edge with the usual $(i \pm 1, j)$ and $(i, j \pm 1)$. An example of such a grid is shown in Figure 1. Even on rectangular grids, the control-volume mixed finite element method can be more accurate than finite differences. However, its main advantage is that it can be applied in a simple, straightforward way to obtain accurate results on irregular grids, allowing the permeability coefficient to be anisotropic and discontinuous. Formulations in common use in the petroleum industry, such as corner-point geometry [18], are well-known to be inconsistent on general logically rectangular grids. Since the motivation for irregular grids is the accuracy of the discretization, such formulations are best limited to careful, restricted use in practice.

We describe the method for rectangular grids in Section 2, and for irregular quadrilateral grids in Section 3. The method is presented in the context of a model pressure equation. Section 4 contains results from numerical experiments, including a comparison to block-centered finite differences and numerical convergence results. Section 5 is a summary.

We conclude this introductory section with brief descriptions of mixed and control-volume finite element methods, two methods that provide some of the building blocks for the

control-volume mixed finite element method. Between these descriptions we also summarize some other methods recently proposed for irregular grids in porous media. These other methods share our goal of circumventing the inconsistencies of approaches such as corner-point geometry.

Mixed finite element methods. We recall some of the essentials of mixed finite-element methods. The idea is to represent a partial differential equation as a system of lower-order equations, solving these for multiple variables of physical interest. To keep the description simple, assume incompressible single-phase flow, neglecting gravitational effects, so that the pressure equation takes the form

$$-\nabla \cdot \left(\frac{k}{\mu} \nabla p \right) = q, \quad \mathbf{x} \in \Omega, \quad (1)$$

where k (scalar or anisotropic tensor) is the permeability, μ the fluid viscosity, p the pressure, q a source/sink (e.g., well) term, and Ω is the reservoir with boundary $\partial\Omega$. Also for simplicity, take the no-flow boundary condition

$$\nabla p \cdot \mathbf{n} = 0, \quad \mathbf{x} \in \partial\Omega. \quad (2)$$

A mixed method separates Darcy's law,

$$\mathbf{v} = -\frac{k}{\mu} \nabla p, \quad (3)$$

where \mathbf{v} is the velocity vector, from conservation of mass,

$$\nabla \cdot \mathbf{v} = q, \quad (4)$$

and solves the system Eqs. (3)–(4) for \mathbf{v} and p , instead of solving Eq. (1) for p and applying Eq. (3) to obtain \mathbf{v} .

For the standard (not control-volume) mixed method, following [19], write Eq. (3) in the form $(\mu/k)\mathbf{v} + \nabla p = 0$, multiply by a vector test function \mathbf{w} , integrate over Ω , and integrate by parts to obtain

$$\int_{\Omega} \frac{\mu}{k} \mathbf{v} \cdot \mathbf{w} \, d\mathbf{x} - \int_{\Omega} \nabla \cdot \mathbf{w} \, p \, d\mathbf{x} = 0. \quad (5)$$

Multiply Eq. (4) by a scalar test function z and integrate over Ω to see that

$$\int_{\Omega} \nabla \cdot \mathbf{v} \, z \, d\mathbf{x} = \int_{\Omega} q \, z \, d\mathbf{x}. \quad (6)$$

The requirements of \mathbf{w} and z are that z and the components of \mathbf{w} be square-integrable, that the divergence $\nabla \cdot \mathbf{w}$ be square-integrable, and that $\mathbf{w} \cdot \mathbf{n} = 0$ on the boundary $\partial\Omega$. At this point, the differential equations are still being viewed continuously, with p and \mathbf{v} satisfying the same conditions as z and \mathbf{w} , respectively.

In two dimensions, the discrete Raviart-Thomas elements can be rectangles or triangles. In either case, for the lowest-order elements that are analogous to block-centered finite

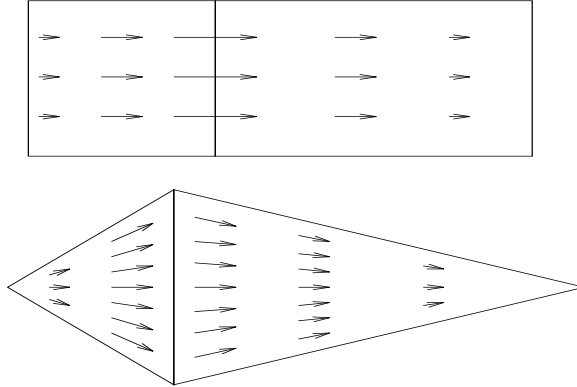


Figure 2: Velocity basis functions on rectangles and triangles

differences, p and z are piecewise-constant. The velocity functions \mathbf{v} and \mathbf{w} can best be viewed by associating a degree of freedom with the flux (normal component times edge length) on each inter-block edge; this covers both the rectangles and the triangles. Velocity functions for which the flux is 1 on one edge (hence the normal component is $1/|E|$, where $|E|$ is the length of the edge) and 0 on other edges are pictured in Figure 2. Fluxes vary linearly in the direction of the velocity. Continuity of flux is assured in either case.

There are two principal advantages to this approach. First, with piecewise-constant z , Eq. (6) yields conservation of mass on an element-by-element basis, in analogy with block-centered finite differences. Second, approximating \mathbf{v} directly by finite elements can be much more accurate than solving for p and invoking Eq. (3), especially when the mobility k/μ is not smooth. An example of the importance of this appears in [11], where a mixed method avoided spurious viscous fingering effects that had appeared in Galerkin finite-element results for miscible displacement. On standard grids, a mixed method has also reduced numerical dispersion in an industry simulator [10]. For standard grids, the convergence and accuracy of these mixed methods are well-established, both independently [19] and as part of a coupled system for miscible displacement [15]. This theory extends in a straightforward way to a grid of parallelograms, which are linear images of rectangles.

For arbitrary quadrilateral grids, Raviart and Thomas [19] and Thomas [23] defined appropriate pressure and velocity spaces via the Piola mapping (see Section 3.1). Stability and convergence were demonstrated more recently by Wang and Mathew [25] and Shen [22]. These error estimates are of significant interest mathematically, but of limited practical value in the geological context motivating our work, because they depend on continuity of the normal and tangential components of \mathbf{v} at an interface; at interfaces where k is discontinuous, the tangential component of \mathbf{v} will also be discontinuous. Farmer *et al.* [12] have applied these methods to petroleum reservoir simulation.

Other methods for irregular grids. In the petroleum industry, Aavatsmark *et al.* [1, 2] have proposed and tested a block-centered finite-difference method involving partitioned fluxes between subdivisions of irregular blocks. The objective is continuity of pressure

and velocity with suitable interpolation between nodes; this would be overdetermined, so some constraints are relaxed. Of a similar flavor is a method proposed and analyzed by Thomas and Trujillo [24], which is a mixed discretization with Eq. (3) written in the form $\mathbf{v} + (k/\mu)\nabla p = 0$ instead of $(\mu/k)\mathbf{v} + \nabla p = 0$. In both methods there is, in essence, a dual velocity grid whose blocks are associated with the corners of pressure blocks. In contrast, as Sections 2 and 3 will show, our velocity grid elements (control volumes) are associated with the edges (or faces in three dimensions) of pressure blocks, as are the velocity degrees of freedom (e.g., Figure 2). We also retain the integration of k^{-1} as in Eq. (5), which will generalize the usual harmonic averaging of k in a simple way.

An expanded mixed method, reducible to a finite-difference scheme by low-order integration, has been formulated, analyzed, and tested by Arbogast *et al.* [3, 4]. The method is expanded in the sense that it introduces an additional variable corresponding to ∇p , subsequently eliminating it under some circumstances. A key to the method is the assumption that there is a global C^2 mapping from the irregular grid to a regular grid, which is not the case for a grid such as that in Figure 1. At non-smooth grid interfaces, or at interfaces with coefficient discontinuities, the method must introduce Lagrange multipliers that correspond physically to pressures on block edges (faces in three dimensions). With these Lagrange multipliers, the method obtains numerically the theoretical convergence rate of $h^{3/2}$ for velocities at midpoints of edges [3], where h is the grid size. The method and its theory are based on the framework of standard mixed methods. Our method, based on the alternative control-volume framework, is considerably simpler, as its degrees of freedom are merely the block pressures and the edge fluxes, with no Lagrange multipliers. Edge pressure values (analogous to Lagrange multipliers) do appear in the derivation in Section 3.2, but they are eliminated before the final system of equations is reached. The resulting method shows a convergence rate of h^2 for velocities (fluxes across edges) in all of the tests performed so far (e.g., those in Section 4), except where the solution is singular.

Control volume finite elements. To obtain a local discrete Darcy law and to avoid the complexities that appear to be necessary with standard mixed methods, we consider procedures based on control-volume finite-element methods [5, 17]. Such schemes have been considered in the petroleum literature [14, 20, 13], but only in a “point-centered” framework. This means that mass conservation is not enforced on the blocks designated by the user, but rather on dual blocks centered about the vertices of the user blocks. Since the vertices are presumably often located at geological interfaces, and since the designated blocks may be of significance to the user, the most desirable approach would be one that conserves mass on the user blocks.

We briefly summarize the point-centered approach. If Eq. (1) is integrated over a volume (area in two dimensions) V and the Gauss divergence theorem is applied, we obtain

$$-\int_{\partial V} \frac{k}{\mu} \nabla p \cdot \mathbf{n} \, ds = \int_V q \, d\mathbf{x}, \quad (7)$$

where ∂V is the boundary of V and ds is the measure on ∂V . A mesh of triangles is defined, where p will be computed at the vertices. With each vertex, one associates a control volume, usually found by taking the Voronoi volume bounded by the perpendicular bisectors of the sides of the triangles. Then Eq. (7) is posed for each control volume, where p is linearly

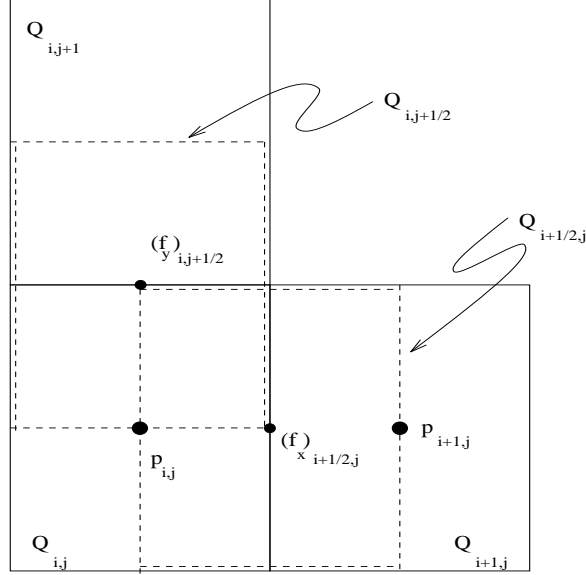


Figure 3: Unknowns and control volumes for rectangular grid

interpolated from the vertices to the interior of each triangle. Thus, p is represented by a standard finite-element shape function, but instead of integrating against the usual weighting functions one integrates over control volumes. This is equivalent to integrating against weighting functions that are 1 on one control volume and 0 on the others. Convergence theories [6, 8] exist for quite general triangulations.

2 Rectangular Grid

We formulate a control-volume mixed finite-element procedure for the system Eqs. (3)–(4), using appropriate shape functions to represent the solution and integrating over appropriate control volumes. We first illustrate this for a rectangular grid, where the details are straightforward and we can use Raviart-Thomas elements as described above.

In Figure 3, we show typical unknowns and control volumes. Let

$$\begin{aligned} Q_{i,j} &= (x_{i-1/2}, x_{i+1/2}) \times (y_{j-1/2}, y_{j+1/2}), \\ Q_{i+1/2,j} &= (x_i, x_{i+1}) \times (y_{j-1/2}, y_{j+1/2}), \\ Q_{i,j+1/2} &= (x_{i-1/2}, x_{i+1/2}) \times (y_j, y_{j+1}), \end{aligned}$$

where (x_i, y_j) is the center of the block $Q_{i,j}$. As in the standard mixed method, we associate pressure unknowns $p_{i,j}$ with block centers (x_i, y_j) , and a flux unknown (normal component of \mathbf{v} times cross-sectional area or length) with each face (edge in two dimensions). On a vertical edge centered at $(x_{i+1/2}, y_j)$, the normal component is the x -component, so we can

denote the unknown by $(f_x)_{i+1/2,j}$. Similarly, on a horizontal edge centered at $(x_i, y_{j+1/2})$, we associate $(f_y)_{i,j+1/2}$. The natural control volumes corresponding to $p_{i,j}$, $(f_x)_{i+1/2,j}$, and $(f_y)_{i,j+1/2}$, respectively, are $Q_{i,j}$, $Q_{i+1/2,j}$, and $Q_{i,j+1/2}$, as seen in Figure 3. From a physical point of view, we can think of $Q_{i+1/2,j}$ as a ‘‘tank’’ with pressures $p_{i,j}$ and $p_{i+1,j}$ imposed at the two ends, and similarly for $Q_{i,j+1/2}$.

We wish to integrate Eq. (3) over control volumes to obtain local discrete Darcy laws on the ‘‘tanks.’’ Note that Eq. (3) is a vector equation that can be resolved into the two components

$$\lambda^{-1}v_x + \frac{\partial p}{\partial x} = 0, \quad (8)$$

$$\lambda^{-1}v_y + \frac{\partial p}{\partial y} = 0, \quad (9)$$

where $\lambda = k/\mu$. We integrate Eq. (8) and Eq. (9) over $Q_{i+1/2,j}$ and $Q_{i,j+1/2}$, respectively, because these equations involve v_x and v_y . Integrating out the partial derivatives of p , this yields

$$\int_{x_i}^{x_{i+1}} \int_{y_{j-1/2}}^{y_{j+1/2}} \lambda^{-1}v_x(x, y) dy dx + \int_{y_{j-1/2}}^{y_{j+1/2}} (p(x_{i+1}, y) - p(x_i, y)) dy = 0, \quad (10)$$

$$\int_{y_j}^{y_{j+1}} \int_{x_{i-1/2}}^{x_{i+1/2}} \lambda^{-1}v_y(x, y) dx dy + \int_{x_{i-1/2}}^{x_{i+1/2}} (p(x, y_{j+1}) - p(x, y_j)) dx = 0. \quad (11)$$

Using the shape functions for p , v_x , and v_y as described above, the integrals in Eqs. (10)–(11) are readily expressed in terms of the unknowns $p_{i,j}$, $p_{i+1,j}$, $p_{i,j+1}$, $(f_x)_{i-1/2,j}$, $(f_x)_{i+1/2,j}$, $(f_x)_{i+3/2,j}$, $(f_y)_{i,j-1/2}$, $(f_y)_{i,j+1/2}$, and $(f_y)_{i,j+3/2}$. We then obtain the discrete Darcy equations on the ‘‘tanks’’: in the x -direction on $Q_{i+1/2,j}$,

$$a_{i+1/2,j;i-1/2,j}(f_x)_{i-1/2,j} + a_{i+1/2,j;i+1/2,j}(f_x)_{i+1/2,j} + a_{i+1/2,j;i+3/2,j}(f_x)_{i+3/2,j} + p_{i+1,j} - p_{i,j} = 0, \quad (12)$$

where

$$a_{i+1/2,j;i-1/2,j} = \frac{1}{8} \frac{\lambda_{i,j}^{-1}}{|Q_{i,j}|} (x_{i+1/2} - x_{i-1/2})^2, \quad (13)$$

$$a_{i+1/2,j;i+1/2,j} = \frac{3}{8} \frac{\lambda_{i,j}^{-1}}{|Q_{i,j}|} (x_{i+1/2} - x_{i-1/2})^2 + \frac{3}{8} \frac{\lambda_{i+1,j}^{-1}}{|Q_{i+1,j}|} (x_{i+3/2} - x_{i+1/2})^2, \quad (14)$$

$$a_{i+1/2,j;i+3/2,j} = \frac{1}{8} \frac{\lambda_{i+1,j}^{-1}}{|Q_{i+1,j}|} (x_{i+3/2} - x_{i+1/2})^2, \quad (15)$$

and in the y -direction on $Q_{i,j+1/2}$,

$$a_{i,j+1/2;i,j-1/2}(f_y)_{i,j-1/2} + a_{i,j+1/2;i,j+1/2}(f_y)_{i,j+1/2} + a_{i,j+1/2;i,j+3/2}(f_y)_{i,j+3/2} + p_{i,j+1} - p_{i,j} = 0, \quad (16)$$

where coefficients in Eq. (16) are obtained by equations analogous to Eqs. (13)–(15). On each block $Q_{i,j}$, p is constant, f_x varies linearly with x and is constant in y , and f_y is constant in x and varies linearly with y .

We also integrate Eq. (4), this time over the control volumes $Q_{i,j}$. Applying the Gauss divergence theorem to convert the left-hand side into a boundary integral (four edge integrals), we have

$$\begin{aligned} & \int_{y_{j-1/2}}^{y_{j+1/2}} v_x(x_{i+1/2}, y) dy - \int_{y_{j-1/2}}^{y_{j+1/2}} v_x(x_{i-1/2}, y) dy + \int_{x_{i-1/2}}^{x_{i+1/2}} v_y(x, y_{j+1/2}) dx \\ & - \int_{x_{i-1/2}}^{x_{i+1/2}} v_y(x, y_{j-1/2}) dx = \int_{y_{j-1/2}}^{y_{j+1/2}} \int_{x_{i-1/2}}^{x_{i+1/2}} q(x, y) dx dy. \end{aligned} \quad (17)$$

Again, the integrals are expressed in terms of $(f_x)_{i-1/2,j}$, $(f_x)_{i+1/2,j}$, $(f_y)_{i,j-1/2}$, and $(f_y)_{i,j+1/2}$, yielding the discrete mass conservation:

$$(f_x)_{i-1/2,j} - (f_x)_{i+1/2,j} + (f_y)_{i,j-1/2} - (f_y)_{i,j+1/2} = -|Q_{i,j}|q_{i,j}. \quad (18)$$

Eqs. (12), (16), and (18) thus give rise to a symmetric system of linear equations that is solved for the pressures at block centers and the fluxes across edges:

$$\begin{bmatrix} \mathbf{M}_x & 0 & \mathbf{N}_x \\ 0 & \mathbf{M}_y & \mathbf{N}_y \\ \mathbf{N}_x^T & \mathbf{N}_y^T & 0 \end{bmatrix} \begin{bmatrix} f_x \\ f_y \\ p \end{bmatrix} = \begin{bmatrix} 0 \\ 0 \\ -|Q|q \end{bmatrix}, \quad (19)$$

where \mathbf{M}_x is tridiagonal (for unknown ordering by horizontal rows, so that $(i-1/2, j)$, $(i+1/2, j)$, $(i+3/2, j)$ are consecutive), \mathbf{M}_y is tridiagonal (ordering by vertical columns so that $(i, j-1/2)$, $(i, j+1/2)$, $(i, j+3/2)$ are consecutive) and each row of \mathbf{N}_x and \mathbf{N}_y contains one +1 and one -1, corresponding to the two adjacent block pressures.

It is instructive to relate this control-volume mixed finite-element method to the familiar block-centered finite-difference approach. Eq. (17) would be the usual block-centered mass-balance equation if the normal velocities on edges were given by discrete pressure gradients multiplied by harmonically averaged mobilities. Examining Eqs. (10)–(11), we see that this would be the case if the v_x and v_y integrals approximated v_x and v_y by constants on their respective control volumes (or, equivalently, if a midpoint integration rule were used). In matrix terms, \mathbf{M}_x and \mathbf{M}_y would become diagonal, so the system would have the form

$$\begin{bmatrix} \mathbf{M}' & \mathbf{N} \\ \mathbf{N}^T & 0 \end{bmatrix} \begin{bmatrix} f \\ p \end{bmatrix} = \begin{bmatrix} 0 \\ -|Q|q \end{bmatrix}, \quad (20)$$

with \mathbf{M}' diagonal, and elimination of f would yield

$$\mathbf{N}^T \mathbf{M}'^{-1} \mathbf{N} p = |Q|q. \quad (21)$$

This demonstrates the close relationship between the control-volume mixed method and block-centered finite differences. Both methods involve local mass conservation and a local

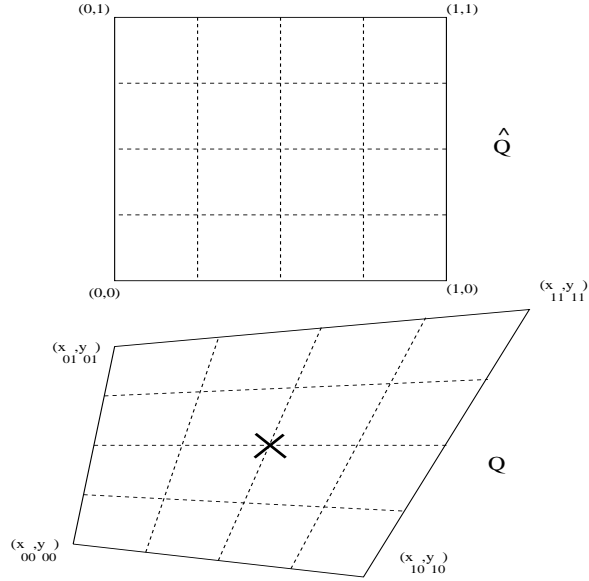


Figure 4: Reference quadrilateral \hat{Q} and quadrilateral Q

Darcy law. The mixed method’s higher-order approximation of v_x and v_y , each varying linearly in its own direction, couples the velocities in Eqs. (10)–(11) and makes the methods different. This increases the accuracy of the solution (for example, see Problem 1 of Section 4), but makes it more expensive to solve the discrete system.

It is also useful, for the sake of generalization to irregular grids, to take a vector point of view of Eqs. (10)–(11). In passing from Eq. (3) to Eq. (8), we took the x -component of Eq. (3); this is equivalent to taking the dot product of Eq. (3) with the unit vector $\mathbf{x} = (1, 0)$. In Eq. (10) we restricted the integration to the control volume $Q_{i+1/2,j}$. Thus, we can obtain Eq. (10) by taking the dot product of Eq. (3) with a vector field that is \mathbf{x} on $Q_{i+1/2,j}$ and zero elsewhere, then integrating over Ω . This vector field is the finite-element vector “test function” corresponding to Eq. (10). Similarly, Eq. (11) relates to a vector test function that is $\mathbf{y} = (0, 1)$ on $Q_{i,j+1/2}$ and zero elsewhere. This perspective seems pointless on a rectangular grid, where components are easy to work with, but it will be helpful otherwise.

3 Irregular Quadrilateral Grid

With the rectangular case as a guide, we develop a formulation for general quadrilaterals. One important step is to be able to relate a general quadrilateral to a reference one. Consider the quadrilateral Q in Figure 4, which is assumed to have vertices at (x_{00}, y_{00}) , (x_{01}, y_{01}) , (x_{10}, y_{10}) , and (x_{11}, y_{11}) . Let the reference quadrilateral \hat{Q} be the unit square. There is a

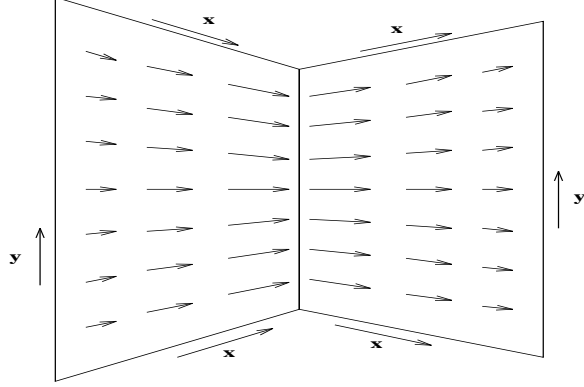


Figure 5: Velocity basis function on quadrilaterals

unique bilinear mapping of \hat{Q} onto Q that sets up coordinates on Q :

$$\begin{aligned} x(\hat{x}, \hat{y}) &= x_{00} + (x_{10} - x_{00})\hat{x} + (x_{01} - x_{00})\hat{y} \\ &\quad + (x_{11} - x_{10} - x_{01} + x_{00})\hat{x}\hat{y}, \end{aligned} \quad (22)$$

$$\begin{aligned} y(\hat{x}, \hat{y}) &= y_{00} + (y_{10} - y_{00})\hat{x} + (y_{01} - y_{00})\hat{y} \\ &\quad + (y_{11} - y_{10} - y_{01} + y_{00})\hat{x}\hat{y}. \end{aligned} \quad (23)$$

The resulting coordinate lines are as depicted in Fig. 4. The pressure in Q is associated with the image of the center of \hat{Q} , i.e., with the node $(x(\frac{1}{2}, \frac{1}{2}), y(\frac{1}{2}, \frac{1}{2}))$ indicated by \times in the figure. Note that this is not generally the centroid of Q . As long as Q is a *convex* quadrilateral (all angles less than 180 degrees), the bilinear mapping has an inverse. We assume henceforth that the quadrilaterals are convex so that for each $(x, y) \in Q$ the inverse mapping gives an associated $(\hat{x}, \hat{y}) \in \hat{Q}$. There is thus a one-to-one correspondence between points in the physical space Q and the reference space \hat{Q} .

3.1 Shape functions and unknowns

Now consider the extension of the control-volume mixed formulation to general quadrilaterals. To maintain continuity of flux, we want the normal component of a velocity function to be constant on each edge. Then we can associate degrees of freedom with fluxes on edges, as in the rectangle and triangle cases. In Figure 5 we show two adjacent quadrilaterals with the coordinates determined by the mapping Eqs. (22)–(23). The velocity vector function that has normal component $1/|E|$ on the common edge of length $|E|$ (hence has flux 1) and 0 on the other edges is pictured. It is oriented along, say, x -coordinate lines, and has constant normal component on each complementary y -line, with the magnitude of the flux varying linearly in the x -direction. We now describe this vector function analytically.

First we identify significant directions in the quadrilateral. Referring to Eqs. (22)–(23),

define

$$\begin{aligned}\mathbf{X}(\hat{x}, \hat{y}) &= \left(\frac{\partial x}{\partial \hat{x}}, \frac{\partial y}{\partial \hat{x}} \right) \\ &= (x_{10} - x_{00} + (x_{11} - x_{10} - x_{01} + x_{00})\hat{y}, \\ &\quad y_{10} - y_{00} + (y_{11} - y_{10} - y_{01} + y_{00})\hat{y}),\end{aligned}\tag{24}$$

$$\begin{aligned}\mathbf{Y}(\hat{x}, \hat{y}) &= \left(\frac{\partial x}{\partial \hat{y}}, \frac{\partial y}{\partial \hat{y}} \right) \\ &= (x_{01} - x_{00} + (x_{11} - x_{10} - x_{01} + x_{00})\hat{x}, \\ &\quad y_{01} - y_{00} + (y_{11} - y_{10} - y_{01} + y_{00})\hat{x}).\end{aligned}\tag{25}$$

These can be viewed as the images of the vectors $(1, 0)$ and $(0, 1)$, respectively, under the mapping from \hat{Q} to Q . We have defined them for (\hat{x}, \hat{y}) in the reference quadrilateral, but because of the one-to-one correspondence mentioned previously, we can just as well consider them defined for (x, y) in the physical quadrilateral. In the physical space, they point in the directions of the coordinate lines pictured in Figure 4. However, they are not unit vectors; their length depends on the size of Q and they have the dimensions of length. Define also the corresponding unit vectors and normal vectors:

$$\mathbf{x} = \frac{\left(\frac{\partial x}{\partial \hat{x}}, \frac{\partial y}{\partial \hat{x}} \right)}{\left[\left(\frac{\partial x}{\partial \hat{x}} \right)^2 + \left(\frac{\partial y}{\partial \hat{x}} \right)^2 \right]^{1/2}}\tag{26}$$

$$\mathbf{y} = \frac{\left(\frac{\partial x}{\partial \hat{y}}, \frac{\partial y}{\partial \hat{y}} \right)}{\left[\left(\frac{\partial x}{\partial \hat{y}} \right)^2 + \left(\frac{\partial y}{\partial \hat{y}} \right)^2 \right]^{1/2}}\tag{27}$$

$$\mathbf{n}_x = \frac{\left(\frac{\partial y}{\partial \hat{y}}, -\frac{\partial x}{\partial \hat{y}} \right)}{\left[\left(\frac{\partial x}{\partial \hat{y}} \right)^2 + \left(\frac{\partial y}{\partial \hat{y}} \right)^2 \right]^{1/2}}\tag{28}$$

$$\mathbf{n}_y = \frac{\left(-\frac{\partial y}{\partial \hat{x}}, \frac{\partial x}{\partial \hat{x}} \right)}{\left[\left(\frac{\partial x}{\partial \hat{x}} \right)^2 + \left(\frac{\partial y}{\partial \hat{x}} \right)^2 \right]^{1/2}}\tag{29}$$

Here \mathbf{x} and \mathbf{y} are unit vectors in the directions of \mathbf{X} and \mathbf{Y} , respectively, \mathbf{n}_x is a unit vector normal to \mathbf{Y} , and \mathbf{n}_y is a unit vector normal to \mathbf{X} . Figure 5 shows \mathbf{x} and \mathbf{y} , while Figure 6 shows \mathbf{n}_x and \mathbf{n}_y .

Returning to the vector function \mathbf{v} in Figure 5, let Q be the left-hand quadrilateral. To evaluate \mathbf{v} at (x, y) , first use the inverse mapping to find the corresponding (\hat{x}, \hat{y}) . Then $\mathbf{v}(x, y)$ is the vector in the direction of \mathbf{X} whose \mathbf{n}_x -component (i.e., $\mathbf{v} \cdot \mathbf{n}_x$) is equal to $\hat{x}/\|\mathbf{Y}\|$ (so that the flux across the “vertical” line through (x, y) is \hat{x}). After some manipulation,

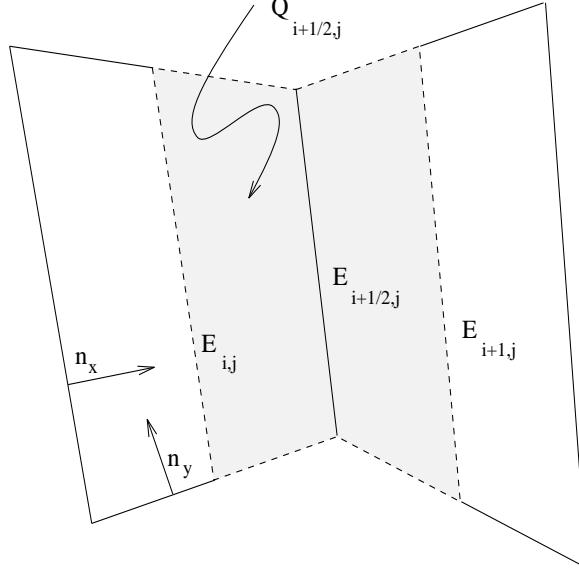


Figure 6: Control-volume mixed finite elements on quadrilaterals

one can show that this is given by

$$\mathbf{v}(x, y) = \frac{\hat{x}\mathbf{X}}{J(\hat{x}, \hat{y})}, \quad (30)$$

where

$$\begin{aligned} J(\hat{x}, \hat{y}) &= \frac{\partial x}{\partial \hat{x}} \frac{\partial y}{\partial \hat{y}} - \frac{\partial x}{\partial \hat{y}} \frac{\partial y}{\partial \hat{x}} \\ &= [(x_{10} - x_{00})(y_{01} - y_{00}) - (x_{01} - x_{00})(y_{10} - y_{00})] \\ &\quad + [(x_{10} - x_{00})(y_{11} - y_{01}) - (x_{11} - x_{01})(y_{10} - y_{00})]\hat{x} \\ &\quad + [(x_{11} - x_{10})(y_{01} - y_{00}) - (x_{01} - x_{00})(y_{11} - y_{10})]\hat{y} \end{aligned} \quad (31)$$

is the Jacobian of the mapping in Eqs. (22)–(23) from \hat{Q} to Q . Note that $J(\hat{x}, \hat{y}) = \|\mathbf{X}\|\|\mathbf{Y}\|\sin\theta$, where θ is the angle between \mathbf{X} and \mathbf{Y} . For a rectangular grid, this angle is 90 degrees, so that $\mathbf{n}_x = \mathbf{x}$ and we obtain $\mathbf{v}(x, y) = \hat{x}\mathbf{x}/\|\mathbf{Y}\|$, as we would expect. In the right-hand quadrilateral, everything is the same except that $1 - \hat{x}$ replaces \hat{x} . Similar expressions hold for a velocity basis function corresponding to a “horizontal” edge, with \hat{x} , \mathbf{X} , and \mathbf{x} replaced by \hat{y} , \mathbf{Y} , and \mathbf{y} , respectively.

The unknowns that we use to describe the velocity are the fluxes across edges, namely $|E_{i+1/2,j}|(\mathbf{v} \cdot \mathbf{n}_x)_{i+1/2,j}$ and $|E_{i,j+1/2}|(\mathbf{v} \cdot \mathbf{n}_y)_{i,j+1/2}$, which we abbreviate to $(f_x)_{i+1/2,j}$ and $(f_y)_{i,j+1/2}$ in analogy with the rectangular case. These velocity shape functions and unknowns can be obtained from those on rectangles by a so-called Piola transformation [7].

For pressure, the natural choice of shape functions is still piecewise constants, introducing no additional complications, and the unknowns are $p_{i,j}$ as in the rectangular case.

3.2 Test functions and control volumes

To obtain discrete equations from which we can solve for pressures at block centers and fluxes across edges, we must choose suitable control volumes and mimic the integrations leading to Eqs. (10)–(11) and (17). For the integrations of Eq. (3), we use images of rectangular control volumes $Q_{i+1/2,j}$ and $Q_{i,j+1/2}$ under the mapping in Eqs. (22)–(23). This is pictured in Figure 6, where the control volume associated with the common edge consists of the image of $(\frac{1}{2}, 1) \times (0, 1)$ under the mapping to the left-hand quadrilateral and the image of $(0, \frac{1}{2}) \times (0, 1)$ under the mapping to the right-hand quadrilateral. In physical space, this can be described by taking the midpoints of the four edges adjacent to the common edge in question, then joining the two pairs of midpoints by line segments. We denote such control volumes by $Q_{i+1/2,j}$ and $Q_{i,j+1/2}$, as we did previously for the rectangular grid. $Q_{i+1/2,j}$ in Figure 6 will be the “tank” with pressures $p_{i,j}$ and $p_{i+1,j}$ at the two ends. For the integrations of Eq. (4), we simply take the quadrilateral blocks $Q_{i,j}$ as control volumes.

Continuity equation. For the integrations, we also require test functions. For Eq. (4), these are simply scalar characteristic functions of the control volumes, i.e., functions that are 1 on one volume and zero elsewhere. If we denote the edges of $Q_{i,j}$ by $E_{i+1/2,j}$, etc., and integrate Eq. (4) over the control volume, the Gauss divergence theorem (using the fact that the normal velocity component is constant on each edge) yields

$$\begin{aligned} (\mathbf{v} \cdot \mathbf{n}_x)_{i+1/2,j} |E_{i+1/2,j}| - (\mathbf{v} \cdot \mathbf{n}_x)_{i-1/2,j} |E_{i-1/2,j}| + (\mathbf{v} \cdot \mathbf{n}_y)_{i,j+1/2} |E_{i,j+1/2}| \\ - (\mathbf{v} \cdot \mathbf{n}_y)_{i,j-1/2} |E_{i,j-1/2}| = \int_{Q_{i,j}} q \, dz, \end{aligned} \quad (32)$$

so that Eq. (18) is obtained for quadrilaterals as well as rectangles, where dz is the two-dimensional measure on $Q_{i,j}$. The equation is easily incorporated into the discrete system as before.

Darcy equation. For Eq. (3), the situation is more complicated. On the rectangular grid, the test function given by \mathbf{x} on $Q_{i+1/2,j}$ and zero elsewhere allowed the x -partial derivative of p to be integrated out, leaving integrals of p on lines that were interior to the constant-pressure blocks. This is the desired outcome, and we show how to achieve this on a general quadrilateral grid.

Let $Q_{i+1/4,j}$ and $Q_{i+3/4,j}$ denote the “left-hand half” and “right-hand half,” respectively, of $Q_{i+1/2,j}$. Then $Q_{i+1/4,j}$ is the image of the right-hand half, $(1/2, 1) \times (0, 1)$, of \hat{Q} under the mapping Eqs. (22)–(23). Using \mathbf{X} as the test function, the p integral analogous to the one in Eq. (10) is

$$\begin{aligned} \int_{Q_{i+1/4,j}} \nabla p \cdot \mathbf{X} \, dz &= \int_{Q_{i+1/4,j}} \left(\frac{\partial p}{\partial x} \frac{\partial x}{\partial \hat{x}} + \frac{\partial p}{\partial y} \frac{\partial y}{\partial \hat{x}} \right) dz \\ &= \int_{Q_{i+1/4,j}} \frac{\partial p}{\partial \hat{x}} dz \end{aligned}$$

$$\begin{aligned}
&= \int_0^1 \int_{1/2}^1 \frac{\partial p}{\partial \hat{x}} J d\hat{x} d\hat{y} \\
&= \int_0^1 \int_{1/2}^1 \left(\frac{\partial}{\partial \hat{x}} (pJ) - p \frac{\partial J}{\partial \hat{x}} \right) d\hat{x} d\hat{y}, \tag{33}
\end{aligned}$$

where $J = J_{i,j}$ is the Jacobian of the mapping from \hat{Q} to $Q_{i,j}$, as in Eq. (31). Since J is linear in \hat{x} , $\partial J/\partial \hat{x} = b$ is constant, and Eq. (33) becomes

$$\begin{aligned}
\int_{Q_{i+1/4,j}} \nabla p \cdot \mathbf{X} dz &= \int_0^1 [J(1, \hat{y})p(1, \hat{y}) - J(1/2, \hat{y})p(1/2, \hat{y})] d\hat{y} \\
&\quad - \frac{\partial J}{\partial \hat{x}} \int_0^1 \int_{1/2}^1 p d\hat{x} d\hat{y}. \tag{34}
\end{aligned}$$

Now we suppose that p is approximated by a linear (not bilinear) polynomial in \hat{x} and \hat{y} , an approximation of error $O(h^2)$, where h is the diameter of $Q_{i+1/4,j}$. This will allow us to reduce the above expression to an appropriate numerical scheme. Since J is also linear, the Jp integrals can be evaluated by Simpson's rule in \hat{y} :

$$\begin{aligned}
\int_0^1 J(1, \hat{y})p(1, \hat{y}) d\hat{y} &= \frac{1}{6}J(1, 0)p(1, 0) + \frac{2}{3}J(1, 1/2)p(1, 1/2) \\
&\quad + \frac{1}{6}J(1, 1)p(1, 1), \\
\int_0^1 J(1/2, \hat{y})p(1/2, \hat{y}) d\hat{y} &= \frac{1}{6}J(1/2, 0)p(1/2, 0) + \frac{2}{3}J(1/2, 1/2)p(1/2, 1/2) \\
&\quad + \frac{1}{6}J(1/2, 1)p(1/2, 1). \tag{35}
\end{aligned}$$

For the p integral, we use the trapezoidal rule in \hat{x} and Simpson's rule (higher order than necessary, but easier to combine with the other terms) in \hat{y} :

$$\begin{aligned}
\frac{\partial J}{\partial \hat{x}} \int_0^1 \int_{1/2}^1 p d\hat{x} d\hat{y} &= \frac{1}{24} \frac{\partial J}{\partial \hat{x}} (p(1/2, 0) + p(1, 0)) + \frac{1}{6} \frac{\partial J}{\partial \hat{x}} (p(1/2, 1/2) + p(1, 1/2)) \\
&\quad + \frac{1}{24} \frac{\partial J}{\partial \hat{x}} (p(1/2, 1) + p(1, 1)). \tag{36}
\end{aligned}$$

Substituting Eqs. (35)–(36) into Eq. (34) and collecting coefficients, we have

$$\begin{aligned}
\int_{Q_{i+1/4,j}} \nabla p \cdot \mathbf{X} dz &= \left(\frac{1}{6}J(1, 0) - \frac{1}{24} \frac{\partial J}{\partial \hat{x}} \right) p(1, 0) \\
&\quad - \left(\frac{1}{6}J(1/2, 0) + \frac{1}{24} \frac{\partial J}{\partial \hat{x}} \right) p(1/2, 0) \\
&\quad + \left(\frac{2}{3}J(1, 1/2) - \frac{1}{6} \frac{\partial J}{\partial \hat{x}} \right) p(1, 1/2)
\end{aligned}$$

$$\begin{aligned}
& - \left(\frac{2}{3}J(1/2, 1/2) + \frac{1}{6} \frac{\partial J}{\partial \hat{x}} \right) p(1/2, 1/2) \\
& + \left(\frac{1}{6}J(1, 1) - \frac{1}{24} \frac{\partial J}{\partial \hat{x}} \right) p(1, 1) \\
& - \left(\frac{1}{6}J(1/2, 1) + \frac{1}{24} \frac{\partial J}{\partial \hat{x}} \right) p(1/2, 1) \\
= & \frac{1}{6}J(3/4, 0)(p(1, 0) - p(1/2, 0)) \\
& + \frac{2}{3}J(3/4, 1/2)(p(1, 1/2) - p(1/2, 1/2)) \\
& + \frac{1}{6}J(3/4, 1)(p(1, 1) - p(1/2, 1)), \tag{37}
\end{aligned}$$

where the last step uses the linearity of J with respect to \hat{x} . With p being linear, $\partial p / \partial \hat{x}$ is constant, so that the three p differences just obtained are all equal; hence, using the linearity of J with respect to \hat{y} , Eq. (37) reduces to

$$\int_{Q_{i+1/4,j}} \nabla p \cdot \mathbf{X} dz = J_{i,j}(3/4, 1/2)(p_{i+1/2,j} - p_{i,j}), \tag{38}$$

recalling that $p_{i,j} = p(1/2, 1/2)$ and letting $p_{i+1/2,j} = p(1, 1/2)$ be a pressure value on the edge $E_{i+1/2,j}$. The value $p_{i+1/2,j}$ is not one of the desired block-center pressure unknowns and we wish to eliminate it. A similar derivation for $Q_{i+3/4,j}$ leads to

$$\int_{Q_{i+3/4,j}} \nabla p \cdot \mathbf{X} dz = J_{i+1,j}(1/4, 1/2)(p_{i+1,j} - p_{i+1/2,j}). \tag{39}$$

Hence, by choosing the test vector field

$$\mathbf{w}_{i+1/2,j} = \begin{cases} \mathbf{X} / J_{i,j}(3/4, 1/2) & \text{on } Q_{i+1/4,j}, \\ \mathbf{X} / J_{i+1,j}(1/4, 1/2) & \text{on } Q_{i+3/4,j}, \\ \mathbf{0} & \text{elsewhere,} \end{cases} \tag{40}$$

we combine constant multiples of Eqs. (38)–(39) into

$$\int_{Q_{i+1/2,j}} \nabla p \cdot \mathbf{w}_{i+1/2,j} dz = p_{i+1,j} - p_{i,j}, \tag{41}$$

and the edge value $p_{i+1/2,j}$ has been eliminated. Note that we did not have to require that p be piecewise constant in this derivation, though we will generally think of the numerical approximation of p in this way.

The step just completed is the elimination of the analogues of the Lagrange multipliers of Arbogast *et al.* [3, 4], mentioned in the discussion of other methods for irregular grids in Section 1. The ability to carry out this step is a special property of the control-volume mixed method, as opposed to the standard framework in which the vector shape and test

functions are the same. In the latter case, the test function must have continuous normal flux, and there is no freedom to choose weights as in Eq. (40) above. There is no physical reason for this constraint (unlike flux continuity for the shape functions), which is an artifact of the numerical approach. The control-volume formulation allows (indeed, compels) flux discontinuities in the test functions.

At this point we have chosen a test function and have integrated the p term of Eq. (3). For the \mathbf{v} term, we consider

$$\begin{aligned} \int_{\Omega} \Lambda^{-1} \mathbf{v} \cdot \mathbf{w}_{i+1/2,j} dz &= \int_{Q_{i+1/4,j}} \Lambda_{i,j}^{-1} \mathbf{v} \cdot \mathbf{X} / J_{i,j}(3/4, 1/2) dz \\ &\quad + \int_{Q_{i+3/4,j}} \Lambda_{i+1,j}^{-1} \mathbf{v} \cdot \mathbf{X} / J_{i+1,j}(1/4, 1/2) dz, \end{aligned} \quad (42)$$

where Λ may be a full anisotropic tensor. To find the desired coefficients, write

$$\begin{aligned} \mathbf{v} &= (f_x)_{i-1/2,j} \mathbf{v}_{i-1/2,j} + (f_x)_{i+1/2,j} \mathbf{v}_{i+1/2,j} + (f_x)_{i+3/2,j} \mathbf{v}_{i+3/2,j} \\ &\quad + (f_y)_{i,j+1/2} \mathbf{v}_{i,j+1/2} + (f_y)_{i,j-1/2} \mathbf{v}_{i,j-1/2} \\ &\quad + (f_y)_{i+1,j+1/2} \mathbf{v}_{i+1,j+1/2} + (f_y)_{i+1,j-1/2} \mathbf{v}_{i+1,j-1/2} \\ &\quad + \text{other terms}, \end{aligned} \quad (43)$$

where (for example) $\mathbf{v}_{i+1/2,j}$ is the velocity field with flux 1 across $E_{i+1/2,j}$ and 0 across all other edges. Then, substituting for \mathbf{v} , we obtain the discrete Darcy equation analogous to Eq. (12)

$$\begin{aligned} &a_{i+1/2,j;i-1/2,j} (f_x)_{i-1/2,j} + a_{i+1/2,j;i+1/2,j} (f_x)_{i+1/2,j} + a_{i+1/2,j;i+3/2,j} (f_x)_{i+3/2,j} \\ &\quad + a_{i+1/2,j;i,j+1/2} (f_y)_{i,j+1/2} + a_{i+1/2,j;i,j-1/2} (f_y)_{i,j-1/2} \\ &\quad + a_{i+1/2,j;i+1,j+1/2} (f_y)_{i+1,j+1/2} + a_{i+1/2,j;i+1,j-1/2} (f_y)_{i+1,j-1/2} \\ &\quad + p_{i+1,j} - p_{i,j} = 0, \end{aligned} \quad (44)$$

where (for example in analogy with Eq. (14))

$$\begin{aligned} a_{i+1/2,j;i+1/2,j} &= \int_{Q_{i+1/4,j}} \Lambda_{i,j}^{-1} \mathbf{v}_{i+1/2,j} \cdot \mathbf{X} / J_{i,j}(3/4, 1/2) dz \\ &\quad + \int_{Q_{i+3/4,j}} \Lambda_{i+1,j}^{-1} \mathbf{v}_{i+1/2,j} \cdot \mathbf{X} / J_{i+1,j}(1/4, 1/2) dz. \end{aligned} \quad (45)$$

To evaluate the $Q_{i+1/4,j}$ integral in Eq. (45), first note that $\mathbf{v}_{i+1/2,j}$ is parallel to \mathbf{X} . Thus, the unit vectors $\mathbf{v}_{i+1/2,j} / \|\mathbf{v}_{i+1/2,j}\|$ and $\mathbf{X} / \|\mathbf{X}\|$ point in the same direction, and are therefore equal. Also note that $J = \|\mathbf{X}\| \|\mathbf{Y}\| (\mathbf{v}_{i+1/2,j} \cdot \mathbf{n}_x) / \|\mathbf{v}_{i+1/2,j}\|$, because the angle θ between \mathbf{X} and \mathbf{Y} (hence between $\mathbf{v}_{i+1/2,j}$ and \mathbf{Y}) is the complement of the angle η between $\mathbf{v}_{i+1/2,j}$ and \mathbf{n}_x , so that $\sin \theta = \cos \eta = (\mathbf{v}_{i+1/2,j} \cdot \mathbf{n}_x) / \|\mathbf{v}_{i+1/2,j}\|$. Furthermore, $\|\mathbf{Y}\| (\mathbf{v}_{i+1/2,j} \cdot \mathbf{n}_x)$ is the flux that varies linearly across $Q_{i+1/4,j}$, being equal to 1 at the

right edge and $1/2$ at the left (the “vertical” center line of $Q_{i,j}$); hence, the flux is equal to \hat{x} . Finally, recall that $\mathbf{A}\mathbf{v} \cdot \mathbf{w} = \mathbf{v} \cdot \mathbf{A}^T \mathbf{w}$ if \mathbf{A} is a square matrix with transpose \mathbf{A}^T . Thus:

$$\begin{aligned}
\int_{Q_{i+1/4,j}} \Lambda_{i,j}^{-1} \mathbf{v}_{i+1/2,j} \cdot \mathbf{X} dz &= \int_{Q_{i+1/4,j}} \|\mathbf{v}_{i+1/2,j}\| \frac{\mathbf{v}_{i+1/2,j}}{\|\mathbf{v}_{i+1/2,j}\|} \cdot (\Lambda_{i,j}^{-1})^T \mathbf{X} dz \\
&= \int_{Q_{i+1/4,j}} \frac{\|\mathbf{X}\| \|\mathbf{Y}\| (\mathbf{v}_{i+1/2,j} \cdot \mathbf{n}_x)}{J} \frac{\mathbf{X}}{\|\mathbf{X}\|} \cdot (\Lambda_{i,j}^{-1})^T \mathbf{X} dz \\
&= \int_{Q_{i+1/4,j}} \|\mathbf{Y}\| (\mathbf{v}_{i+1/2,j} \cdot \mathbf{n}_x) (\Lambda_{i,j}^{-1} \mathbf{X}) \cdot \mathbf{X} \frac{1}{J} dz \\
&= \int_0^1 \int_{1/2}^1 \hat{x} (\Lambda_{i,j}^{-1} \mathbf{X}) \cdot \mathbf{X} d\hat{x} d\hat{y}, \tag{46}
\end{aligned}$$

where the last step is a change of variable. Similarly, we find that

$$\int_{Q_{i+3/4,j}} \Lambda_{i+1,j}^{-1} \mathbf{v}_{i+1/2,j} \cdot \mathbf{X} dz = \int_0^1 \int_0^{1/2} (1 - \hat{x}) (\Lambda_{i+1,j}^{-1} \mathbf{X}) \cdot \mathbf{X} d\hat{x} d\hat{y}. \tag{47}$$

Hence, combining Eqs. (45)–(47),

$$\begin{aligned}
a_{i+1/2,j;i+1/2,j} &= \frac{1}{J_{i,j}(3/4, 1/2)} \int_0^1 \int_{1/2}^1 \hat{x} (\Lambda_{i,j}^{-1} \mathbf{X}) \cdot \mathbf{X} d\hat{x} d\hat{y} \\
&\quad + \frac{1}{J_{i+1,j}(1/4, 1/2)} \int_0^1 \int_0^{1/2} (1 - \hat{x}) (\Lambda_{i+1,j}^{-1} \mathbf{X}) \cdot \mathbf{X} d\hat{x} d\hat{y}. \tag{48}
\end{aligned}$$

Next, consider $\mathbf{v}_{i-1/2,j}$ in order to obtain $a_{i+1/2,j;i-1/2,j}$ in analogy with Eq. (13). Of the two “halves” $Q_{i+1/4,j}$ and $Q_{i+3/4,j}$ where $\mathbf{w}_{i+1/2,j}$ does not vanish, $\mathbf{v}_{i-1/2,j}$ is nonzero only on $Q_{i+1/4,j}$. Reasoning as above,

$$a_{i+1/2,j;i-1/2,j} = \frac{1}{J_{i,j}(3/4, 1/2)} \int_0^1 \int_{1/2}^1 (1 - \hat{x}) (\Lambda_{i,j}^{-1} \mathbf{X}) \cdot \mathbf{X} d\hat{x} d\hat{y}. \tag{49}$$

Similarly, $\mathbf{v}_{i+3/2,j}$ is nonzero only on $Q_{i+3/4,j}$, and Eq. (15) has the analogue

$$a_{i+1/2,j;i+3/2,j} = \frac{1}{J_{i+1,j}(1/4, 1/2)} \int_0^1 \int_0^{1/2} \hat{x} (\Lambda_{i+1,j}^{-1} \mathbf{X}) \cdot \mathbf{X} d\hat{x} d\hat{y}. \tag{50}$$

The logic is slightly different if the term for a horizontal edge, e.g. $\mathbf{v}_{i,j+1/2}$ to obtain $a_{i+1/2,j;i,j+1/2}$, is considered. These terms were 0 in the rectangular case. Here again only one of the “halves” is relevant, in this case $Q_{i+1/4,j}$. Now $\mathbf{v}_{i,j+1/2}$ is parallel to \mathbf{Y} , so that $\mathbf{v}_{i,j+1/2} / \|\mathbf{v}_{i,j+1/2}\| = \mathbf{Y} / \|\mathbf{Y}\|$, and $J = \|\mathbf{X}\| \|\mathbf{Y}\| (\mathbf{v}_{i,j+1/2} \cdot \mathbf{n}_y) / \|\mathbf{v}_{i,j+1/2}\|$; also, $\|\mathbf{X}\| (\mathbf{v}_{i,j+1/2} \cdot \mathbf{n}_y) = \hat{y}$. Then Eq. (46) is replaced by

$$\int_{Q_{i+1/4,j}} \Lambda_{i,j}^{-1} \mathbf{v}_{i,j+1/2} \cdot \mathbf{X} dz = \int_{Q_{i+1/4,j}} \|\mathbf{v}_{i,j+1/2}\| \frac{\mathbf{Y}}{\|\mathbf{Y}\|} \cdot (\Lambda_{i,j}^{-1})^T \mathbf{X} dz$$

$$\begin{aligned}
&= \int_{Q_{i+1/4,j}} \|\mathbf{X}\|(\mathbf{v}_{i,j+1/2} \cdot \mathbf{n}_y)(\Lambda_{i,j}^{-1} \mathbf{Y}) \cdot \mathbf{X} \frac{1}{J} dz \\
&= \int_0^1 \int_{1/2}^1 \hat{y}(\Lambda_{i,j}^{-1} \mathbf{Y}) \cdot \mathbf{X} d\hat{x} d\hat{y}, \tag{51}
\end{aligned}$$

so that

$$a_{i+1/2,j;i,j+1/2} = \frac{1}{J_{i,j}(3/4, 1/2)} \int_0^1 \int_{1/2}^1 \hat{y}(\Lambda_{i,j}^{-1} \mathbf{Y}) \cdot \mathbf{X} d\hat{x} d\hat{y}. \tag{52}$$

By analogous steps, the other three coefficients are:

$$a_{i+1/2,j;i,j-1/2} = \frac{1}{J_{i,j}(3/4, 1/2)} \int_0^1 \int_{1/2}^1 (1-\hat{y})(\Lambda_{i,j}^{-1} \mathbf{Y}) \cdot \mathbf{X} d\hat{x} d\hat{y}, \tag{53}$$

$$a_{i+1/2,j;i+1,j+1/2} = \frac{1}{J_{i+1,j}(1/4, 1/2)} \int_0^1 \int_0^{1/2} \hat{y}(\Lambda_{i+1,j}^{-1} \mathbf{Y}) \cdot \mathbf{X} d\hat{x} d\hat{y}, \tag{54}$$

$$a_{i+1/2,j;i+1,j-1/2} = \frac{1}{J_{i+1,j}(1/4, 1/2)} \int_0^1 \int_0^{1/2} (1-\hat{y})(\Lambda_{i+1,j}^{-1} \mathbf{Y}) \cdot \mathbf{X} d\hat{x} d\hat{y}. \tag{55}$$

This completes the description of the Darcy equation for the vertical edge $E_{i+1/2,j}$. The Darcy equation for the horizontal edge $E_{i,j+1/2}$,

$$\begin{aligned}
&a_{i,j+1/2;i,j-1/2}(f_y)_{i,j-1/2} + a_{i,j+1/2;i,j+1/2}(f_y)_{i,j+1/2} + a_{i,j+1/2;i,j+3/2}(f_y)_{i,j+3/2} \\
&+ a_{i,j+1/2;i+1/2,j}(f_x)_{i+1/2,j} + a_{i,j+1/2;i-1/2,j}(f_x)_{i-1/2,j} \\
&+ a_{i,j+1/2;i+1/2,j+1}(f_x)_{i+1/2,j+1} + a_{i,j+1/2;i-1/2,j+1}(f_x)_{i-1/2,j+1} \\
&+ p_{i,j+1} - p_{i,j} = 0, \tag{56}
\end{aligned}$$

is derived in a completely analogous fashion. The coefficients are defined by equations similar to Eqs. (48)–(50) and (52)–(55).

Assuming that the reciprocal mobility Λ^{-1} is a constant tensor on each grid block, the integrals in the a coefficients are straightforward to evaluate analytically. The dot products in these integrals are simply quadratic polynomials in \hat{x} and \hat{y} (total degree 2, so that the highest-order terms are \hat{x}^2 , $\hat{x}\hat{y}$, \hat{y}^2). Explicit expressions for the a -coefficients can be found in [21]. These can be evaluated once and stored for use throughout the life of the grid block in the simulation. Even in multiphase or variable-viscosity flow, where Λ^{-1} is time-dependent, the dependence is restricted to a scalar multiple of the tensor, so that the above double integrals can be stored and later multiplied by a variable scalar.

3.3 Discrete system of linear equations

The discrete system of the control-volume mixed finite element method, with irregular quadrilateral grid and full anisotropic tensor permeability, consists of “vertical”-edge Darcy Eq. (44), “horizontal”-edge Darcy Eq. (56), and continuity Eq. (18). The non-symmetric

linear system can be written in the form

$$\begin{bmatrix} \mathbf{M}_{xx} & \mathbf{M}_{xy} & \mathbf{N}_x \\ \mathbf{M}_{yx} & \mathbf{M}_{yy} & \mathbf{N}_y \\ \mathbf{N}_x^T & \mathbf{N}_y^T & 0 \end{bmatrix} \begin{bmatrix} f_x \\ f_y \\ p \end{bmatrix} = \begin{bmatrix} 0 \\ 0 \\ -|Q|q \end{bmatrix}, \quad (57)$$

where \mathbf{M}_{xx} and \mathbf{M}_{yy} are tridiagonal with the same nonzero pattern as in the rectangular case Eq. (19) (though with different values), and \mathbf{N}_x and \mathbf{N}_y have the same ± 1 entries as in Eq. (19). \mathbf{M}_{xy} and \mathbf{M}_{yx} each have four nonzero bands, corresponding to the four nonzero a -coefficients involving $(\Lambda^{-1}\mathbf{Y}) \cdot \mathbf{X}$ for \mathbf{M}_{xy} and $(\Lambda^{-1}\mathbf{X}) \cdot \mathbf{Y}$ for \mathbf{M}_{yx} .

Note that the a -coefficients in Eqs. (48)–(50), (52)–(55) amalgamate the complexities of distorted grids and of anisotropic tensor permeabilities. With a scalar permeability and an orthogonal grid, one sees that a dot product such as $(\lambda^{-1}\mathbf{X}) \cdot \mathbf{Y}$ vanishes, because $\lambda^{-1}\mathbf{X}$ is parallel to \mathbf{X} (due to the scalar λ^{-1}) and hence perpendicular to \mathbf{Y} (by orthogonality). Then the matrix \mathbf{M} of a -coefficients reduces to tridiagonal form, as observed previously for the rectangular case. If either condition fails to hold, $(\Lambda^{-1}\mathbf{X}) \cdot \mathbf{Y}$ can be nonzero, and additional bands can appear in \mathbf{M} . The nonzero pattern with both distortion and anisotropy is the same as with either one alone. Within the bounds of consistent discretization, the expressions in Eqs. (18), (44), (48)–(50), (52)–(56) seem as simple as one could reasonably hope. Given a tensor Λ^{-1} , there is a theoretical possibility of choosing distorted \mathbf{X} and \mathbf{Y} such that $(\Lambda^{-1}\mathbf{X}) \cdot \mathbf{Y}$ vanishes, resulting in a sparser \mathbf{M} , but the practical significance of this is not clear.

3.4 Extension to Three Dimensions

It is important to realize that the system obtained here on quadrilaterals extends readily in three dimensions to hexalaterals H that are trilinear images of a unit cube $\hat{H} = [0, 1]^3$. The faces of such hexalaterals may not lie in a plane, but this is not a concern in principle because the curvilinear faces, normal vectors, and fluxes are uniquely determined. A “horizontal”-face Darcy equation similar to Eq. (44) or Eq. (56) would have the form

$$\begin{aligned} & a_{i,j,k+1/2;i,j,k+1/2}(f_z)_{i,j,k+1/2} \\ & + a_{i,j,k+1/2;i,j,k-1/2}(f_z)_{i,j,k-1/2} + a_{i,j,k+1/2;i,j,k+3/2}(f_z)_{i,j,k+3/2} \\ & + a_{i,j,k+1/2;i+1/2,j,k}(f_x)_{i+1/2,j,k} + a_{i,j,k+1/2;i-1/2,j,k}(f_x)_{i-1/2,j,k} \\ & + a_{i,j,k+1/2;i+1/2,j,k+1}(f_x)_{i+1/2,j,k+1} + a_{i,j,k+1/2;i-1/2,j,k+1}(f_x)_{i-1/2,j,k+1} \\ & + a_{i,j,k+1/2;i,j+1/2,k}(f_y)_{i,j+1/2,k} + a_{i,j,k+1/2;i,j-1/2,k}(f_y)_{i,j-1/2,k} \\ & + a_{i,j,k+1/2;i,j+1/2,k+1}(f_y)_{i,j+1/2,k+1} + a_{i,j,k+1/2;i,j-1/2,k+1}(f_y)_{i,j-1/2,k+1} \\ & + p_{i,j,k+1} - p_{i,j,k} = 0, \end{aligned} \quad (58)$$

with, for example,

$$\begin{aligned} & a_{i,j,k+1/2;i+1/2,j,k} \\ & = \frac{1}{J_{i,j,k}(1/2, 1/2, 3/4)} \int_{1/2}^1 \int_0^1 \int_0^1 \hat{x}(\Lambda_{i,j,k}^{-1}\mathbf{X}) \cdot \mathbf{Z} \, d\hat{x} \, d\hat{y} \, d\hat{z}. \end{aligned} \quad (59)$$

The Darcy equations for “vertical” faces normal to x -fluxes and y -fluxes would be obtained analogously. The continuity equation would have the form of Eq. (18) with two additional f_z terms, one with each sign. We note that the control-volume mixed finite element method has been used in three-dimensional astrophysical applications [9]. However, only Cartesian grids were considered and the mobility coefficient Λ was constant and scalar.

3.5 Relation to Block-Centered Finite Differences

On rectangles, we saw that the control-volume mixed method reduced to block-centered finite differences if the normal fluxes were constant instead of linearly varying. The equivalent reduction in the present setting is to replace the factors \hat{x} , $1-\hat{x}$, \hat{y} , or $1-\hat{y}$ in Eqs. (48)–(50), (52)–(55) by 1 if they are greater than $1/2$, and by 0 if they are less than $1/2$. Then \mathbf{M}_{xx} and \mathbf{M}_{yy} become diagonal (Eqs. (49)–(50) yield zeros), but \mathbf{M}_{xy} and \mathbf{M}_{yx} do not vanish. This reflects the necessity of retaining cross-derivative information in a consistent approximation when grid distortion or anisotropy is present. The inconsistency of corner-point geometry [18] is a consequence of its suppression of this information, so as to work within a 5-point stencil in two dimensions and a 7-point stencil in three. If distortion and anisotropy are mild, then \mathbf{M} is strongly diagonally dominant, and it should be reasonable to approximate \mathbf{M}^{-1} by a matrix with the same sparsity pattern as \mathbf{M} . The resulting analogue of Eq. (21) would have a 9-point stencil in two dimensions and a 19-point stencil in three, the same connection structure found by Arbogast *et al.* [4]. This has not been implemented at this writing and will not be discussed further here.

4 Results

The control-volume mixed finite element method has been tested on a variety of two-dimensional problems, involving uniform and irregular grids, scalar and tensor permeabilities, and constant and variable permeabilities. The velocities exhibit second-order convergence in all situations except where the exact solution has a singularity, in which case second-order convergence is not possible. Following is a representative sampling of these results. Additional results can be found in [21] and [16].

In most of the test problems, an analytical solution was known. Otherwise, a suitable fine-grid numerical solution was used for this purpose. Let p and (v_x, v_y) denote the exact pressure and velocity, respectively, with P and (V_x, V_y) being the corresponding numerical solutions. In the tables, pressure errors are measured by $e_p = \|p - P\|_{L^2}$, the continuous L^2 norm of the difference. Because P is piecewise constant, first-order convergence is the best that can be expected. Velocity errors are calculated separately for vertical and horizontal edges:

$$e_{v_x} = \left[\sum_{i,j} \left(\int_{E_{i+1/2,j}} (\mathbf{v} - \mathbf{V}) \cdot \mathbf{n}_x ds \right)^2 \right]^{1/2}, \quad (60)$$

Grid	Control Volume Mixed			Finite Difference		
	e_{v_x}	e_{v_y}	$\ \mathbf{e}_v\ $	e_{v_x}	e_{v_y}	$\ \mathbf{e}_v\ $
16×16	1.54E-4	9.41E-5	1.80E-4	5.65E-4	6.51E-4	8.62E-4
32×32	8.50E-5	4.98E-5	9.85E-5	3.30E-4	3.72E-4	4.98E-4
64×64	4.43E-5	2.51E-5	5.09E-5	1.90E-4	2.09E-4	2.82E-4
128×128	1.90E-5	1.06E-5	2.17E-5	1.08E-4	1.17E-4	1.59E-4
256×256	—	—	—	6.35E-5	6.69E-5	9.22E-5

Table 1: Comparison of methods for uniform grids and variable permeability - entire domain

$$e_{v_y} = \left[\sum_{i,j} \left(\int_{E_{i,j+1/2}} (\mathbf{v} - \mathbf{V}) \cdot \mathbf{n}_y ds \right)^2 \right]^{1/2}. \quad (61)$$

Then $\|\mathbf{e}_v\| \equiv (e_{v_x}^2 + e_{v_y}^2)^{1/2}$ is equivalent to a discrete $H(\text{div})$ norm of the vector velocity error (which incorporates the L^2 norms of $(v - V)_x$, $(v - V)_y$, and $\text{div}(\mathbf{v} - \mathbf{V})$, the last of which is zero by the local conservation property of the mixed method).

Problem 1. We first compare the accuracy of the control-volume mixed method with that of block-centered finite differences on rectangular grids. Problem 1 subdivides the domain $\Omega = [-1, 1]^2$ into four quadrants and assigns a different value of λ (a scalar) to each: 0.01 for $x > 0, y > 0$; 0.05 for $x < 0, y > 0$; 10 for $x < 0, y < 0$; 33.33 for $x > 0, y < 0$. The source term was zero over the entire domain and the boundary conditions specified the normal component of the velocity on $\partial\Omega$ as follows:

$$\begin{array}{ll} 2000/1005 & x = -1, y < 0, \\ 10/1005 & x = -1, y > 0, \\ 6666/3334 & x = 1, y < 0, \\ 2/3334 & x = 1, y > 0, \\ 0 & y = \pm 1. \end{array}$$

These boundary conditions specify both the total flux in at the left boundary and out at the right boundary to be equal to 2, and no flow at the top and bottom boundaries. Note that making the x -component of the velocity on the the left and right boundaries proportional to the permeability avoids singularities in the velocities at $(\pm 1, 0)$; however there is still a singularity at the origin. Uniform grids from 16×16 to 256×256 were used. In the absence of an analytical solution, the 256×256 mixed solution was used for comparison. Velocity errors for the two methods are given in Table 1. The superiority of the mixed method is evident; the accuracy of its velocities on a 32×32 grid is similar to finite differences on a 256×256 grid. This is not an artifact of the use of the 256×256 mixed solution as “exact,” since the 128×128 and 256×256 finite difference solutions differ from each other by an order of magnitude more than the corresponding mixed solutions differ from each other.

This is the one instance in which the mixed velocities do not show second-order convergence, the reason being that the true solution has a singularity at the origin. Excluding from the summation in Eq. (60) those edges $E_{i+1/2,j}$ that lie inside $(-\frac{1}{8}, \frac{1}{8})^2$ (and similarly in

Grid	Control Volume Mixed			Finite Difference		
	ϵ_{v_x}	ϵ_{v_y}	$\ \mathbf{e}_v\ $	ϵ_{v_x}	ϵ_{v_y}	$\ \mathbf{e}_v\ $
16×16	1.28E-4	9.12E-5	1.57E-4	5.57E-4	4.95E-4	7.45E-4
32×32	3.69E-5	2.78E-5	4.62E-5	2.61E-4	2.38E-4	3.53E-4
64×64	9.56E-6	7.46E-6	1.21E-5	1.29E-4	1.19E-4	1.75E-4
128×128	2.06E-6	1.64E-6	2.63E-6	6.42E-5	5.99E-5	8.78E-5
256×256	—	—	—	3.22E-5	3.02E-5	4.42E-5

Table 2: Comparison of methods for uniform grids and variable permeability - away from singularity

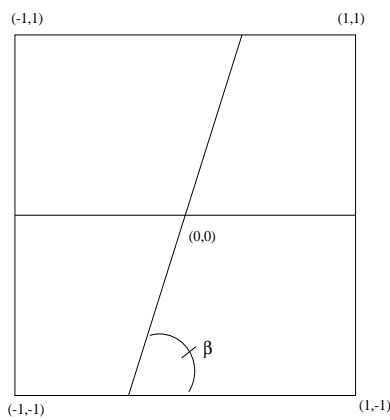


Figure 7: Macro-blocks of distorted grids

Eq. (61) excluding those edges $E_{i,j+1/2}$ that lie inside $(-\frac{1}{8}, \frac{1}{8})^2$ we can see the behavior of the error away from this singularity. Table 2 shows the result when the errors are calculated over $\Omega \setminus (-\frac{1}{8}, \frac{1}{8})^2$, the domain minus a small square centered at the origin. From the table we see that the mixed method is still superior, and that the velocity errors for the mixed method seem to indicate second-order convergence away from the singularity whereas the finite difference velocity errors appear to be first-order convergent.

It should be noted that while this problem demonstrates that the mixed method can produce more accurate velocity approximations than the finite difference method, the two methods exhibit comparable accuracy for the pressure. The remaining problems study the accuracy of the control-volume mixed method under various conditions.

Problem 2. In this problem we study the effect of grid distortion and tensor permeability on the control-volume mixed method. Here the distortion is based on the angle β shown in Figure 7, where finer grids are obtained by refining the four macro-blocks along bilinear coordinate lines. The coefficient Λ , a constant anisotropic tensor, is given by

$$\Lambda = \begin{bmatrix} \cos \theta & \sin \theta \\ -\sin \theta & \cos \theta \end{bmatrix} \begin{bmatrix} 1 & 0 \\ 0 & 0.01 \end{bmatrix} \begin{bmatrix} \cos \theta & -\sin \theta \\ \sin \theta & \cos \theta \end{bmatrix}, \quad (62)$$

	$\beta = 80^\circ, \theta = 0^\circ$		$\beta = 80^\circ, \theta = 45^\circ$	
Grid	e_p	$\ \mathbf{e}_v\ $	e_p	$\ \mathbf{e}_v\ $
16×16	2.506E-1	2.789E-3	2.256E+0	3.337E-1
32×32	1.266E-1	7.414E-4	6.332E-1	1.174E-1
64×64	6.353E-2	1.885E-4	1.736E-1	3.355E-2
128×128	3.189E-2	4.734E-5	5.189E-2	8.740E-3
	$\beta = 60^\circ, \theta = 0^\circ$		$\beta = 60^\circ, \theta = 45^\circ$	
Grid	e_p	$\ \mathbf{e}_v\ $	e_p	$\ \mathbf{e}_v\ $
16×16	2.611E-1	4.400E-3	3.081E+0	5.345E-1
32×32	1.334E-1	1.230E-3	9.405E-1	2.338E-1
64×64	6.970E-2	3.225E-4	2.675E-1	7.644E-2
128×128	3.993E-2	8.208E-5	7.817E-2	2.101E-2

Table 3: Mixed method accuracy for distorted grids, constant tensor permeability

where θ is the angle between the coordinate axes and the principal directions of permeability. No-flow boundary conditions were used and the source term was chosen to yield an exact solution

$$p(x, y) = \cos(\pi x) \cos(2\pi y). \quad (63)$$

Table 3 presents results for the extreme values of θ and several values of β as in Figure 7. The second-order convergence of the velocity is clear, though with $\theta = 45^\circ$ and $\beta = 60^\circ$ (serious anisotropy and distortion) the asymptotic regime is not reached until the grid is quite fine. We note that the accuracy degrades slightly as the grid becomes more distorted, which is no surprise. The degradation of accuracy due to lack of alignment of anisotropy with the grid is much more severe. This effect is greater in this test problem than would be expected in practice, since the 100:1 anisotropy ratio exceeds that of typical porous media, and a modeler would attempt to avoid the worst case of $\theta = 45^\circ$.

Problem 3. The last problem considers a distorted grid, based on the macro-blocks in Figure 8, along with variable tensor permeability. The tensor is given on Regions I, II, and III in Figure 8 by

$$\Lambda_I = \begin{bmatrix} 1/4 & 1/4 \\ 1/4 & 4 \end{bmatrix}, \quad \Lambda_{II} = \begin{bmatrix} 2 & 1 \\ 1 & 1 \end{bmatrix}, \quad \Lambda_{III} = \begin{bmatrix} 2 & 1/2 \\ 1/2 & 1/2 \end{bmatrix}. \quad (64)$$

Boundary conditions and the source term are specified so that the exact solution is

$$p_I(x, y) = x^2 - C, \quad p_{II}(x, y) = \frac{1}{16}y^2 - C, \quad p_{III}(x, y) = \frac{1}{4}y^2 - C, \quad (65)$$

where C is chosen to make the integral of p vanish. The pressure and flux are continuous at interfaces. Table 4 reports the results, and again we see second-order convergence in the velocity.

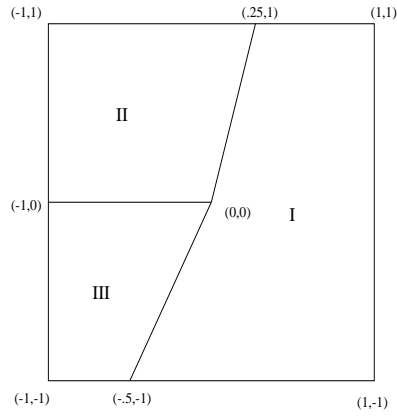


Figure 8: Distorted regions for Problem 6 with variable tensor permeability

Grid	ϵ_p	ϵ_{v_x}	ϵ_{v_y}	$\ \mathbf{e}_v\ $
4×4	2.524E-1	7.226E-3	8.884E-3	1.145E-2
8×8	1.302E-1	1.827E-3	2.580E-3	3.161E-3
16×16	6.578E-2	4.777E-4	6.965E-4	8.445E-4
32×32	3.331E-2	1.264E-4	1.861E-4	2.250E-4
64×64	1.737E-2	3.355E-5	4.984E-5	6.008E-5

Table 4: Mixed method accuracy for distorted grid, variable tensor permeability

5 Conclusions

The control-volume mixed finite element method provides a simple, systematic, easily implemented means of obtaining accurate, locally conservative velocities on irregular block-centered grids, allowing for effects of anisotropy and heterogeneity. Degrees of freedom consist of block pressures and edge (two dimensions) or face (three dimensions) fluxes, with no additional complexities such as Lagrange multipliers, so that the method is strongly analogous to block-centered finite differences from a modeler's point of view. Velocities obey a rigorously derived discrete Darcy law and exhibit second-order convergence as long as the exact solution has no singularities. Heterogeneities and reasonable distortions have only mild effects on the accuracy of the method. Severe anisotropy that is strongly oblique to the coordinates leads to significant increases in velocity errors, though they are still second-order convergent.

The numerical results in Section 4 were obtained using a multilevel solver. The multilevel solver for the discrete control-volume mixed finite element equations is comparable in cost to a typical finite difference solver. This multilevel solver is discussed in [16] and will be the subject of a future paper.

References

- [1] I. Aavatsmark, T. Barkve, Ø. Bøe, and T. Mannseth. Discretization on non-orthogonal, quadrilateral grids for inhomogeneous, anisotropic media. *J. Comp. Phys.*, submitted.
- [2] I. Aavatsmark, T. Barkve, Ø. Bøe, and T. Mannseth. Discretization on unstructured grids for inhomogeneous, anisotropic media, Part I: Derivation of the methods. *SIAM J. Sci. Comput.*, submitted.
- [3] T. Arbogast, P. Keenan, M. Wheeler, and I. Yotov. Logically rectangular mixed methods for Darcy flow on general geometry. In *Proceedings of the 13th SPE Symposium on Reservoir Simulation*, pages 51–59, Dallas, 1995. Society of Petroleum Engineers.
- [4] T. Arbogast, M.F. Wheeler, and I. Yotov. Mixed finite elements for elliptic problems with tensor coefficients as cell-centered finite differences. *SIAM J. Numer. Anal.*, to appear.
- [5] B. R. Baliga and S. V. Patankar. A new finite-element formulation for convection-diffusion problems. *Num. Heat Transfer*, 3:393–409, 1980.
- [6] R. E. Bank and D. J. Rose. Some error estimates for the box method. *SIAM J. Numer. Anal.*, 24:777–787, 1987.
- [7] F. Brezzi and M. Fortin. *Mixed and Hybrid Finite Element Methods*, volume 15 of *Springer Series in Computational Mathematics*. Springer-Verlag, 1991.
- [8] Z. Cai, J. Mandel, and S. F. McCormick. The finite volume element method for diffusion equations on general triangulations. *SIAM J. Numer. Anal.*, 28:392–402, 1991.

- [9] C. Duncan and J. Jones. A mixed method Poisson solver for three-dimensional self-gravitating astrophysical fluid dynamical systems. In N. D. Melson, T. A. Manteuffel, and S. F. McCormick, editors, *Sixth Copper Mountain Conference on Multigrid Methods*, volume CP 3224, pages 159–173, Hampton, VA, 1993. NASA.
- [10] R.E. Ewing and R.F. Heinemann. Incorporation of mixed finite element methods in compositional simulation for reduction of numerical dispersion. In *Proceedings of the 7th SPE Symposium on Reservoir Simulation*, pages 341–347, Dallas, 1983. Society of Petroleum Engineers.
- [11] R.E. Ewing, T.F. Russell, and M.F. Wheeler. Simulation of miscible displacement using mixed methods and a modified method of characteristics. In *Proceedings of the 7th SPE Symposium on Reservoir Simulation*, pages 71–81, Dallas, 1983. Society of Petroleum Engineers.
- [12] C.L. Farmer, D.E. Heath, and D.O. Moody. A global optimization approach to grid generation. In *Proceedings of the 11th SPE Symposium on Reservoir Simulation*, Dallas, 1991. Society of Petroleum Engineers.
- [13] P. A. Forsyth. A control volume finite element method for local mesh refinement. In *Proceedings of the 10th SPE Symposium on Reservoir Simulation*, pages 85–96, Dallas, 1989. Society of Petroleum Engineers.
- [14] Z. E. Heinemann, C. Brand, M. Munka, and Y. M. Chen. Modeling reservoir geometry with irregular grids. In *Proceedings of the 10th SPE Symposium on Reservoir Simulation*, pages 37–54, Dallas, 1989. Society of Petroleum Engineers.
- [15] J. Douglas, Jr., R. E. Ewing, and M. F. Wheeler. Approximation of the pressure by a mixed method in the simulation of miscible displacement. *RAIRO Anal. Numér.*, 17:17–33, 1983.
- [16] J. E. Jones. *A mixed finite volume element method for accurate computation of fluid velocities in porous media*. PhD thesis, University of Colorado at Denver, 1995.
- [17] C. Liu and S.F. McCormick. The finite volume element method (FVE) for planar cavity flow. In *Proceedings of the 11th International Conference on CFD*, Williamsburg, VA, 1988.
- [18] D.K. Ponting. Corner point geometry in reservoir simulation. In P.R. King, editor, *The Mathematics of Oil Recovery*, pages 45–65, Oxford, 1992. Clarendon Press.
- [19] P.A. Raviart and J.M. Thomas. A mixed finite element method for 2nd order elliptic problems. In I. Galligani and E. Magenes, editors, *Mathematical Aspects of Finite Element Methods*, pages 292–315. Springer-Verlag, 1977.
- [20] B. Rozon. A generalized finite volume discretization method for reservoir simulation. In *Proceedings of the 10th SPE Symposium on Reservoir Simulation*, pages 71–84, Dallas, 1989. Society of Petroleum Engineers.

- [21] T.F. Russell. Rigorous block-centered discretizations on irregular grids: Improved simulation of complex reservoir systems. Technical Report No. 3, Project Report, Reservoir Simulation Research Corporation, 1995.
- [22] J. Shen. Mixed finite element methods on distorted rectangular grids. Technical report, Institute for Scientific Computation, Texas A&M University, 1994.
- [23] J.M. Thomas. *Sur l'analyse numerique des methodes d'elements finis hybrides et mixtes*. PhD thesis, Université Pierre et Marie Curie, 1977.
- [24] J.M. Thomas and D. Trujillo. Analysis of finite volume methods. In A.P. Bourgeat, C. Carasso, S. Luckhaus, and A. Mikelić, editors, *Mathematical Modelling of Flow Through Porous Media*, pages 318–336, Singapore, 1995. World Scientific.
- [25] J. Wang and T. Mathew. Mixed finite element methods over quadrilaterals. In *Advances in Numerical Methods & Applications*, pages 203–214. Sofia, 1994.